Journal of Applied Polymer Science

How Does a Polymerized Compounding Affect the Nucleation Effect of a Sorbitol Derivative Nucleating Agent in Isotactic Polypropylene Melt Crystallization?

Qing-Feng Yi, Xiao-Jing Wen, Hui Niu, Jin-Yong Dong

CAS Key Laboratory of Engineering Plastics and State Key Laboratory of Polymer Physics and Chemistry, Joint Laboratory of Polymer Science and Materials, Institute of Chemistry, Chinese Academy of Sciences, Beijing 100190, China

Correspondence to: J.-Y. Dong (E-mail: jydong@iccas.ac.cn)

ABSTRACT: In this article, we investigate the effect of a new polymerized compounding method on the nucleation behavior of a sorbitol derivative nucleating agent for isotactic polypropylene (iPP). This method uses a sorbitol derivative nucleating agent, for example, 1,3: 2,4-dimethylbenzylidene sorbitol (DMBS), which displays itself as aggregated fibrillar crystals, as a support for C_2-symmetric *ansa*-metallocenes best represented by *rac*-$Me_2Si[2\text{-Me-4-Naph-Ind}]_2ZrCl_2$. Activating this DMBS-supported metallocene catalyst with methylaluminoxane, a following *in situ* propylene polymerization results in the formation of iPP/DMBS composition polymers having controllable DMBS concentrations (by virtue of polymerization productivity control), with the DMBS dispersion driven by catalyst fragmentation. Three iPP/DMBS composition polymers having DMBS concentrations of 0.22, 031, and 0.52 wt % were prepared by this means, which, along with their analog melt-mixed counterparts, were subjected to melt crystallization kinetics and crystal morphology studies using differential scanning calorimetry, polarized optical microscopy, and UV–vis spectroscopy. With systematically higher nucleation efficiencies and lower crystallization activation energies, the polymerized iPP/DMBS composition polymers exhibited generally stronger DMBS nucleation effects when compared with their melt-mixed counterparts. Such a benefit was accounted for by a more homogeneous dispersion and better wettability by iPP matrix of DMBS that led to the formation of more nucleation sites and faster crystallization. © 2012 Wiley Periodicals, Inc. J. Appl. Polym. Sci. 000: 000–000, 2012

KEYWORDS: polymerized compounding; sorbitol derivative; isotactic polypropylene

Received 26 October 2010; accepted 30 March 2012; published online
DOI: 10.1002/app.37824

INTRODUCTION

Because of a high price-performance ratio and the highly desirable environmentally benign recyclability, the semicrystalline isotactic polypropylene (iPP) has been one of the most successful members in the family of polymeric materials and is attracting increasing attentions from both industrial and scientific communities aiming at continuously expanding its property envelop to fulfill the ever-growing application demands.[1] Among the many chemical and physical ways to that end, adding a nucleating agent as an additive to effect crystalline infrastructure optimization is an established strategy that is both significant in effect and simple and viable in practice.[2] Different types of nucleating agents exhibit different effects on iPP crystallization[3–7]; nevertheless, it is generally believed that they will raise the crystallization temperature, expedite the overall crystallization process, and reduce crystallite size. In result, both the physical properties including mechanical strengths and optical transparency and processibility will be greatly benefited.

It is a common method to compound iPP/nucleating agent compositions by melt mixing.[8–10] However, the dispersion uniformity of the nucleating agent in iPP matrix is often problematic because of the large chemical polarity gap between the usually highly polar nucleating agent (e.g., sorbitol, the widely used α-nucleating agent) and the nonpolar iPP. A poor dispersion of nucleating agent will unambiguously reduce its efficiency and result in an excess dosage of the relatively high-priced and often hazardous nucleating agent that is certainly undesired by both the compounding manufacturer and the end users. Many efforts have been made to resolve that issue,[11–19] among which excels the polymerized dispersion method that advocates an in-reactor compounding of iPP/nucleating agent compositions.[16,17] Zhang and coworkers reported the first example of polymerization of propylene with a $MgCl_2/TiCl_4$ catalyst in the presence of a

Table I. Characterization of Polymerized (P-Series) and Melt-Mixed (M-Series) MIPP/DMBS Compositions

Sample	DMBS content (wt %)	M_n (g/mol)	M_w/M_n
Neat MIPP[a]	0	6340	3.60
M-1	0.22	6340[a]	3.60
M-2	0.31	6340[a]	3.60
M-3	0.52	6340[a]	3.60
P-1[b]	0.22	6360	3.75
P-2[b]	0.31	6420	3.82
P-3[b]	0.52	6510	3.64

[a]In order to be consistent with the melt-mixed MIPP/DMPS compositions whose preparation underwent a rigorous high-temperature blending that might cause degradation of the MIPP matrix and thus interfere with any comparison made between the two series of MIPP/DMBS compositions as well as with the neat PP, both the neat PP and the polymerized MIPP/DMBS (P-series) compositions were deliberately introduced into the same blending chamber going through the same treatment procedure as those of the melt-mixed MIPP/DMPS (M-series) compositions, [b]These values are only a copy of that of neat PP.

nucleating agent to form nucleated iPP precursors.[16] Although no detailed information was released on both the chemical composition and the dispersion scenario of the nucleating agent, they showed that thus-introduced nucleating agent functioned fairly well in the crystallization process of iPP, with the crystallization rate significantly enhanced and half-time of crystallization, $t_{1/2}$, dramatically shortened compared with those of a nucleating agent-free neat iPP. Besides scientific publications, a number of invention patents disclosed similar techniques as well. Unfortunately, except for almost all positively claiming the viability of fabricating a nucleated iPP precursor using this polymerization technique, no report has ever investigated in detail how and why a polymerized dispersion would affect the efficiency of the nucleation effect of a nucleating agent for iPP melt crystallization.

We recently reported a preparation of iPP/nucleating agent compositions using the *in situ* polymerization approach with a single-site metallocene catalyst.[17] The nucleating agent was a sorbitol compound, 1,3: 2,4-dimethylbenzylidene sorbitol (DMBS), that is a typical member of the most popular family of α-nucleating agents for iPP processing.[18] Our intention to compound the metallocenic iPP (MIPP)/DMBS compositions using the polymerized dispersion method was crystal clear, that is, to combine the advantages of both MIPP of higher grade of clarity than that of Ziegler–Natta iPP and *in situ* polymerization strategy of projected better nucleating agent dispersion and thus higher nucleation efficiency to formulate a better-than-ever transparent iPP recipe. We implemented the idea by supporting *rac*-Me_2Si[2-Me-4-Naph-Ind]$_2ZrCl_2$, one of the so far-reported best single-site catalysts for iPP polymerization, on DMBS crystal aggregate followed by initiating an *in situ* propylene polymerization with the assistant of a cocatalyst of methylaluminoxane (MAO). In the previous report,[17] we showed that the polymerization was of satisfactory yield, and DMBS was well dispersed in MIPP matrix and functioned effectively to lift the crystallization temperature as well as to reduce the crystallite size. Moreover, the polymer product was found to possess a granular morphology, which is highly desirable in view of practical application.

In this article, by comparing to traditional melt-mixed MIPP/DMBS compositions of similar MIPP matrix and DMBS contents, the melt crystallization kinetics and crystal morphology of the above-obtained polymerized MIPP/DMBS compositions are studied at length using differential scanning calorimetry (DSC), polarized optical microscopy (POM), and UV–vis spectroscopy, from where the specific nucleation effect of the polymerization-dispersed DMBS was explored and reasoned on the basis of the nucleation mechanism of a sorbitol nucleating agent.[19]

EXPERIMENTAL

Materials and Instruments

All O_2- and moisture-sensitive manipulations were carried out inside an argon-filled vacuum atmosphere dry box equipped with a dry train. Chemically pure (CP)-grade toluene was deoxygenated by argon purge before refluxing for 48 h and

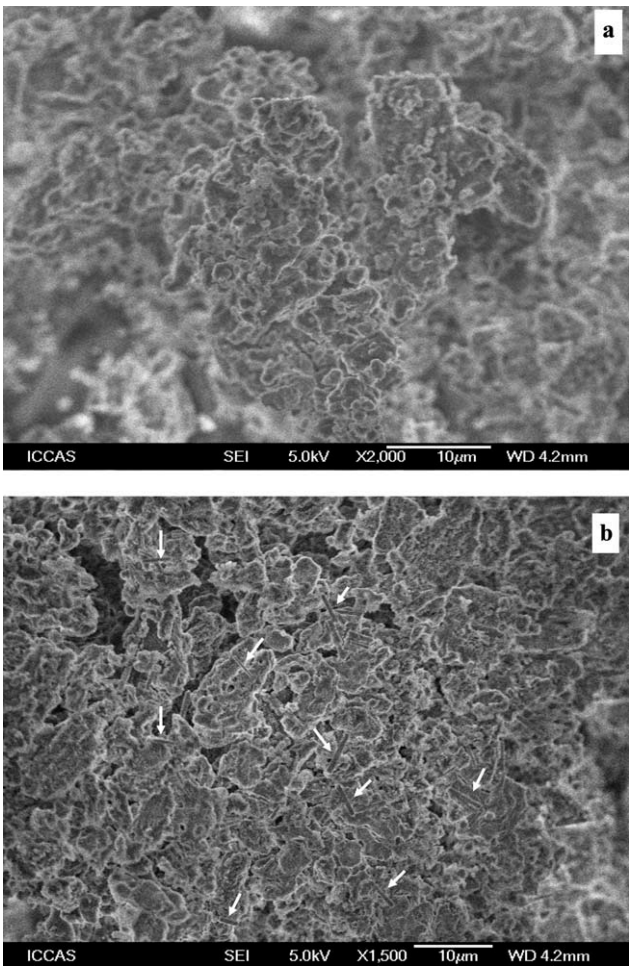

Figure 1. SEM micrographs of the as-polymerized polymer surfaces of (a) the neat MIPP and (b) polymerized MIPP/DMBS composition containing 0.52 wt % of DMBS (sample P-3).

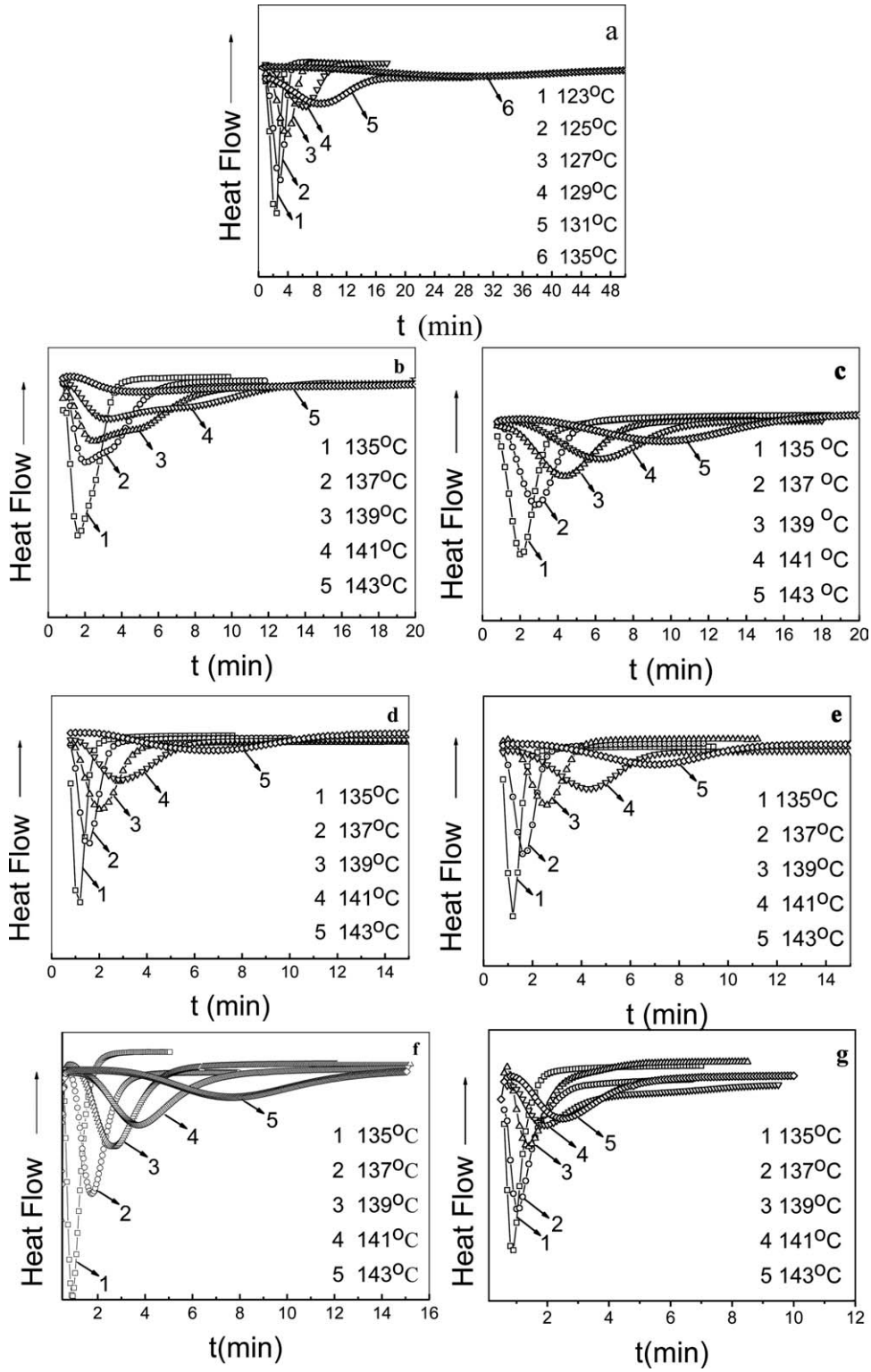

Figure 2. Heat flow as a function of time during the isothermal crystallization at different crystallization temperatures. (a) Neat MIPP, (b) M-1, (c) P-1, (d) M-2, (e) P-2, (f) M-3, and (g) P-3.

distilling over sodium. MAO (10 wt % in toluene) was purchased from Albermarle Company, Baton Rouge, Louisiana, US and used as received. The catalyst, *rac*-Me_2Si(2-Me-4-Naph-Ind)$_2ZrCl_2$, was synthesized according to a published procedure.[20] The nucleating agent, DMBS, was purchased from Shanxi Institute of Chemical Research, Taiyuan, China and recrystallized before use. Polymerization-grade propylene was supplied by Yanshan Petrochemical, Beijing, China.

Applied Polymer SCIENCE

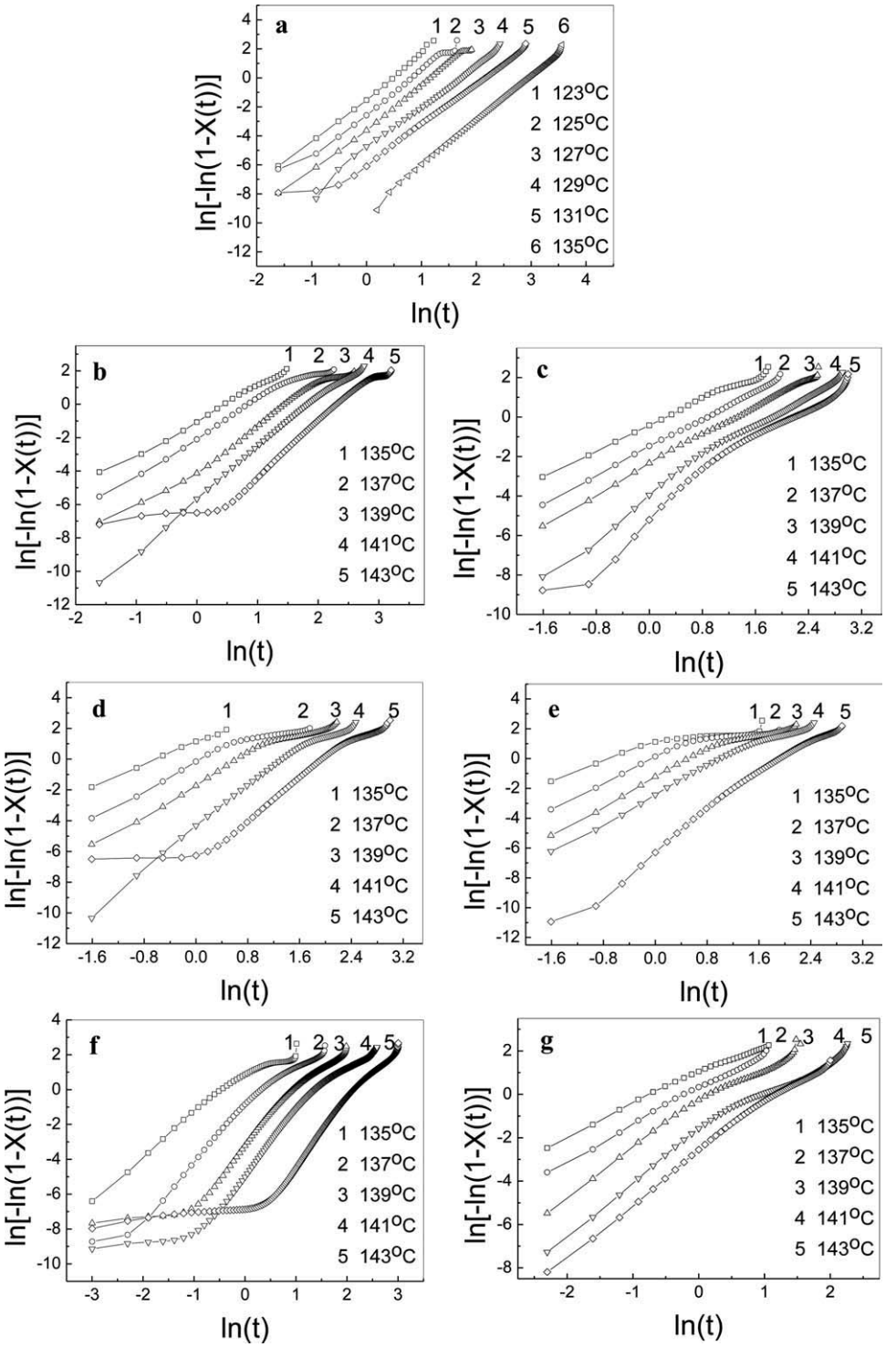

Figure 3. Plots of ln{−ln[1 − $X(t)$]} versus ln(t) at different crystallization temperatures. (a) Neat MIPP, (b) M-1, (c) P-1, (d) M-2, (e) P-2, (f) M-3, and (g) P-3.

All high-temperature ^{1}H-NMR spectra were recorded on a Bruker AM-300 instrument in *o*-dichlorobenzene-d_4 at 110°C. Surface morphology of both the recrystallized nucleating agent and the obtained polymers was examined by scanning electron microscopy (SEM) using a Topcon International Scientific Instruments ISI-SX-40 with secondary electron imaging. Samples were mounted on an aluminum stub and coated with carbon to form a conductive coating. The determination of the melting and crystallization temperatures of the polymers was carried out using DSC with a Perkin-Elmer DSC-7 instrument controller at a heating and cooling rate of 10°C/min. Temperature and calorimetric scales of DSC were calibrated with indium

[T_m = 156°C and melting enthalpy (ΔH_m) = 28.45 J/g]. The DSC measurement was conducted under high-purity (>99.8%) nitrogen protection. Molecular weights and molecular weight distributions of the polymers were determined by gel permeation chromatography (GPC) using a Waters Alliance GPC 2000 instrument equipped with a refractive index detector and a set of μ-Styragel HT columns of 10^6, 10^5, 10^4, and 10^3 pore size in series. The measurement was performed at 150°C with 1,2,4-trichlorobenzene as the eluent with a flow rate of 1.0 mL/min. Narrow molecular weight polystyrene (PS) samples were used as standards for calibration. The crystallite morphology was observed with a POM (Olympus EX51) equipped with a hot-stage device (LTS-350), a temperature controller, and a photocamera (Nikon-800). Before observation, samples were sandwiched between two glass slides. The whole system was heated up to 200°C and held at that temperature for 5 min to erase any thermal history. It was then cooled to 140°C at a rate of 100°C/min. The optical transparency of samples was characterized by a Hitachi UV–Visible (U-3010) scanning spectrophotometer for the injection-molded plaques of 1-mm thickness and 25-mm diameter. Spectrophotometry was performed with λ ranging from 400 to 700 nm. Absorption data acquired at ambient temperature were normalized with respect to the neat iPP. Surface examination of polymer granules was conducted using SEM (Hitachi S-4800, 15 kV). The specimens were prepared by directly coating the as-polymerized polymer samples with Pt.

Preparation of MIPP/DMBS Polymerization Compositions

Before the preparation of MIPP/DMBS polymerization compositions, *rac*-$Me_2Si(2\text{-}Me\text{-}4\text{-}NaphInd)_2ZrCl_2$ catalyst was supported on DMBS crystal aggregate to prepare DMBS-supported catalyst (Zr content at 0.016 mmol/g, procedure described previously).[17] Three MIPP/DMBS compositions containing 0.22, 0.31, and 0.52 wt % of DMBS, respectively, were prepared by *in situ* polymerization with the DMBS-supported catalyst. A typical preparation (MIPP/DMBS composition containing 0.52 wt % of DMBS) procedure is as follows. In a Parr stainless-steel autoclave reactor equipped with a mechanical stirrer was added 0.10 g of DMBS-supported catalyst (0.0016 mmol), 100 mL of toluene, and 1.71 mL (2.40 mmol) of MAO under a propylene pressure of 0.5 MPa. The polymerization temperature was set at 50°C. In half an hour, the reaction was terminated by quenching with 50 mL of acidified ethanol (10%). After filtration, repeated washing with ethanol, and drying at 60°C under vacuum, 11.6 g of polymer was obtained in granular form. The composition of the polymer (DMBS content) was determined by ^{1}H-NMR.

Preparation of MIPP/DMBS Melt-Mixing Compositions

The MIPP matrix for the comparing melt-mixed MIPP/DMBS compositions was prepared by a homogeneous *rac*-$Me_2Si(2\text{-}Me\text{-}4\text{-}Naph\text{-}Ind)_2ZrCl_2$ catalyst and MAO under similar conditions to those for MIPP/DMBS polymerization composition preparation, which was also detailed in the previous report.[17] It is of similar molecular characteristics including molecular weight and molecular weight distribution as those of the MIPP matrixes in the MIPP/DMBS polymerization compositions. This MIPP matrix was melt mixed with fixed amounts of DMBS using a Thermo Haake (Karlsruhe, Germany) extruder operated at 200°C for 5 min to prepare MIPP/DMBS melting–mixing compositions of DMBS loadings at 0.22, 0.31, and 0.52 wt %.

Table II. Parameters for Isothermal Crystallization Kinetics of Neat MIPP and the Two Sets of MIPP/DMBS (Both P- and M-Series) Compositions

Sample	T_c (°C)	K (min^{-n})	$t_{1/2}$ (min)	t_{max} (min)	n
Neat MIPP	123	0.21	1.47	1.49	2.82
	125	0.093	2.05	1.98	2.84
	127	0.0309	2.87	2.81	2.97
	129	0.0086	5.02	4.89	2.71
	131	0.0029	7.71	7.43	2.68
	135	0.000024	27.6	27.2	3.11
M-1	135	0.66	1.05	0.98	2.79
	137	0.23	1.98	1.78	2.78
	139	0.11	3.03	2.96	2.89
	141	0.051	5.18	5.04	3.02
	143	0.032	6.91	6.79	3.14
P-1	135	2.56	0.53	0.49	2.93
	137	0.60	1.21	1.18	3.05
	139	0.33	2.25	2.25	3.11
	141	0.215	3.45	3.47	3.15
	143	0.208	6.73	7.46	3.24
M-2	135	0.86	0.89	0.86	2.90
	137	0.31	1.76	1.75	2.89
	139	0.19	2.87	2.86	2.97
	141	0.076	4.98	4.95	3.07
	143	0.054	6.73	6.71	3.18
P-2	135	2.85	0.31	0.38	2.81
	137	1.35	0.92	0.87	2.95
	139	0.71	1.64	1.58	2.98
	141	0.21	2.51	3.37	3.10
	143	0.16	6.00	6.58	3.21
M-3	135	2.89	0.33	0.37	2.91
	137	1.37	1.02	1.06	2.96
	139	0.75	1.94	1.89	2.88
	141	0.30	2.55	2.51	3.01
	143	0.21	6.03	5.98	3.24
P-3	135	2.91	0.25	0.31	2.84
	137	1.42	0.81	0.75	2.88
	139	0.83	1.41	1.35	2.90
	141	0.28	2.30	2.15	2.93
	143	0.19	5.85	5.75	3.12

Isothermal and Nonisothermal Crystallization Kinetics Studies

Isothermal and nonisothermal crystallization kinetics studies were also conducted using DSC. Each polymer was sampled at 6 mg. The isothermal crystallization kinetics was performed as follows. The sample sealed in an aluminum pan with a diameter of 8 mm was heated up from 50 to 200°C and held at that temperature for 5 min to erase any thermal history. It was then cooled down to a prescribed crystallization temperature at a

cooling rate of 200°C/min. The heat flow as a function of time was recorded. As for the nonisothermal crystallization kinetics, the sample was also heated up to 200°C and held at that temperature for 5 min to eliminate any thermal history. It was then cooled down to 50°C at different cooling rates, i.e., 3, 5, 10, 20, and 50°C/min. The corresponding heat flows were recorded as a function of time.

RESULTS AND DISCUSSION

In this article, we explore whether and why it is advantageous for a sorbitol nucleating agent to be dispersed in iPP matrix via polymerization when compared with the traditional melt-mixing method with respect to its nucleation effect in iPP melt crystallization. For such a purpose, three MIPP/DMBS compositions containing 0.22, 0.31, and 0.52 wt % of DMBS are prepared by *in situ* propylene polymerization using the nucleating agent-supported *rac*-$Me_2Si[2\text{-}Me\text{-}4\text{-}Naph\text{-}Ind]_2ZrCl_2$ catalyst and MAO. This series of nucleated MIPP prototypes are subjected to crystallization behavior study using DSC and POM as well as UV–vis spectrophotometer, and the results of which are compared with those obtained from their melt-mixing counterparts with similar matrix molecular characteristics.

Sample Preparation

The three polymerized MIPP/DMBS composition polymers were prepared from one and the same DMBS-supported *rac*-$Me_2Si[2\text{-}Me\text{-}4\text{-}Naph\text{-}Ind]_2ZrCl_2$ catalyst under otherwise identical polymerization conditions except for varied polymerization durations. The products were collected following a previously described procedure,[17] whose compositions (DMBS contents, wt %) were determined by ^{1}H-NMR and gave values of 0.22, 0.31, and 0.52 wt %. These results are in excellent accordance with those estimated by comparing the original DMBS feeds to the final product weights. Considering a so small quantity each polymer is sampled for ^{1}H-NMR test (ca. 80 mg), this accordance is a good sign heralding a uniform dispersion of DMBS in the composition polymers. With the DMBS contents in the three polymerized composition polymers precisely determined, their melt-mixed counterparts were compounded using a MIPP, a polymer of perfect matrix choice who has similar molecular weight and molecular weight distribution to the polymerized

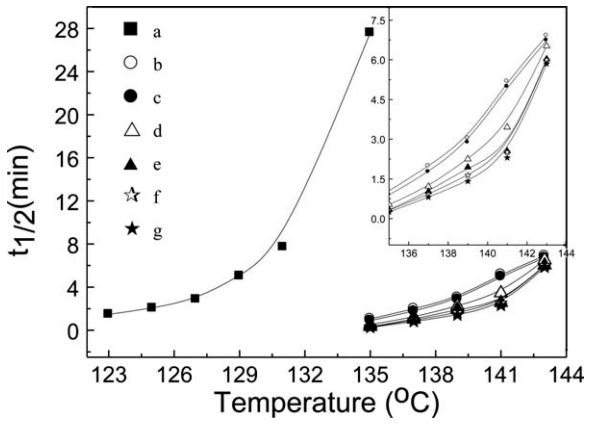

Figure 4. Isothermal crystallization half-time, $t_{1/2}$. (a) Neat MIPP, (b) M-1, (c) P-1, (d) M-2, (e) P-2, (f) M-3, and (g) P-3.

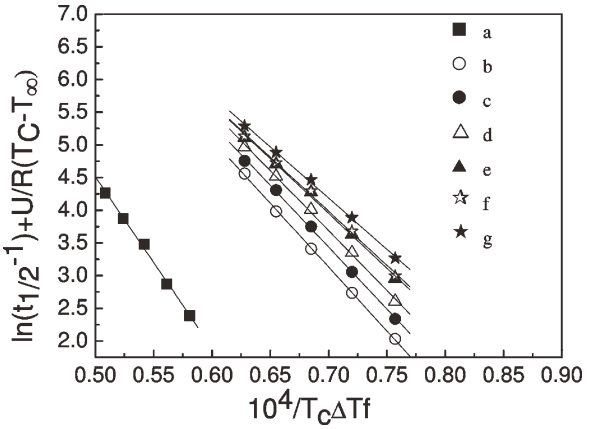

Figure 5. Analysis of the isothermal growth rates as a function of the crystallization temperature based on the Lauritzen–Hoffman secondary nucleation theory. (a) Neat MIPP, (b) M-1, (c) P-1, (d) M-2, (e) P-2, (f) M-3, and (g) P-3.

MIPP/DMBS polymers rendered by a homogeneous *rac*-$Me_2Si[2\text{-}Me\text{-}4\text{-}Naph\text{-}Ind]_2ZrCl_2$/MAO complex, and recrystallized DMBS in a twin-screw extruder operated at 200°C. Table I summarizes the characterization data of the polymerized (P-series) and melt-mixed (M-series) MIPP/DMBS composition polymers as well as the neat MIPP.

Two SEM micrographs of the as-polymerized polymer granules or agglomerates are shown in Figure 1, one [Figure 1(b)] representing the polymerized MIPP/DMBS composition polymer containing 0.52 wt % of DMBS and the other [Figure 1(a)] the neat MIPP. These SEM images render a detailed surface view of the as-polymerized polymer samples. It is very interesting to note that, substantially distinctive from the neat MIPP, the as-polymerized composition polymer surface is sparsely yet discernibly imbedded with topographically random-distributed rod-like DMBS crystals 5–7 μm in length and 0.2–0.5 μm in diameter. It is believable that the finely dispersed nucleating agent will effectively fulfill its nucleating function during the PP matrix melt crystallization.

Melt Crystallization Study Using DSC

Both the two series of MIPP/DMBS composition polymers and the neat MIPP were subjected to crystallization behavior study, first by DSC. Before that, a special treatment was conducted on

Table III. Values of K_g and Chain Folding Free Energy (σ_e) Derived from Isothermal Crystallization of Neat MIPP and the P- and M-Series MIPP/DMBS Composition Samples

Sample entry	k_g (K^2)	σ_e (J/m^2)
Neat MIPP	5.62×10^5	0.096
M-1	3.96×10^5	0.068
P-1	3.85×10^5	0.058
M-2	3.53×10^5	0.049
P-2	3.37×10^5	0.041
M-3	3.85×10^5	0.040
P-3	3.26×10^5	0.038

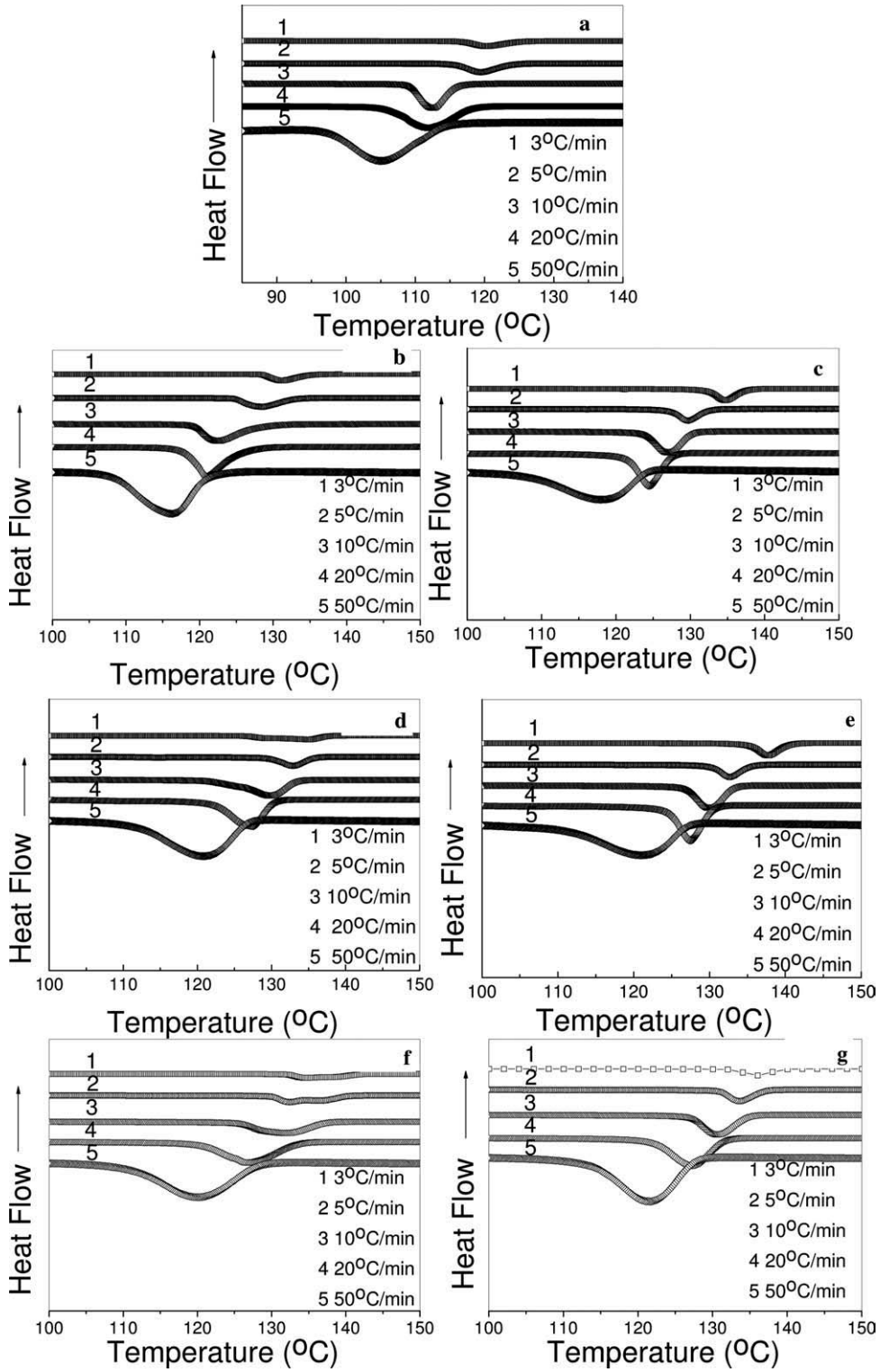

Figure 6. DSC thermograms for nonisothermal crystallization processes of (a) neat MIPP, (b) M-1, (c) P-1, (d) M-2, (e) P-2, (f) M-3, and (g) P-3.

the P-series polymers and neat MIPP by subjecting these polymers to thermoextrusion using the same instrument and following the same procedure as those in the preparation of the M-series composition polymers. This operation was due to the consideration of possible MIPP polymer chain degradation during the high-temperature preparation of the M-series composition polymers that may reduce the comparability between the P- and M-series composition polymers (as well as with the neat MIPP). As the high-temperature extrusion is unavoidable for the M-series polymers' preparation, a same treatment of their

P-series counterparts and the MIPP will compensate the discrepancy.

A standard isothermal crystallization kinetics study was conducted by first choosing five or six different crystallization temperatures. The temperatures for the neat MIPP were set at 123, 125, 127, 129, 131, and 135°C. However, because of the presence of nucleating agent, the two sets of MIPP/DMBS composition polymers were crystallized at much higher temperatures. In view of this, their isothermal crystallization temperatures were chosen to be 135, 137, 139, 141, and 143°C. Figure 2 collects all the recorded DSC scan trails of the isothermal crystallization process.

The isothermal crystallization data were processed using Avrami equation,[21,22]

$$X(t) = 1 - \exp[-K(T)t^n] \tag{1}$$

or

$$\ln\{-\ln[1 - X(t)]\} = n\ln(t) + \ln(K), \tag{2}$$

where $X(t)$, t, K, and n are the relative degree of crystallinity, crystallization time, overall kinetics constant, and Avrami exponent, respectively. The $\ln\{-\ln[1 - X(t)]\}$ versus $\ln(t)$ plots are drawn in Figure 3. Table II summarizes the results derived from the plots, including values of n and k in eqs. (1) and (2) determined from each plot's initial linear sections, and crystallization half-time $t_{1/2}$ defined as the time when the extent of crystallization is 50% completed.

In general, the values of n are not very much different among the neat MIPP and the two sets of MIPP/DMBS composition polymers, indicating all the polymers were crystallized following a normal heterogeneous nucleation plus diffusion-controlled spherulite growth process. However, the crystallization processes were significantly expedited by the nucleating agent. $t_{1/2}$ is plotted against crystallization temperature, as shown in Figure 4. Compared with those of neat MIPP, the $t_{1/2}$ values are significantly reduced in the two MIPP/DMBS composition polymers. These results are consistent with those of the literature findings,[23–25] suggesting the effectiveness of DMBS for PP nucleation.

More interesting $t_{1/2}$ comparisons are made between the two sets of composition polymers. Figure 4 clearly shows that, in the side-by-side comparisons of the $t_{1/2}$ values between the three P-series MIPP/DMBS composition polymers and their corresponding M-series counterparts, the P-series polymers exhibit systematically lower $t_{1/2}$ values, indicating that the P-series composition polymers are prone to faster crystallization.

The crystallization thermodynamics and kinetics were analyzed using Hoffman–Lauritzen secondary nucleation theory,[26–28] where the growth rate of a crystal spherulite G is defined by

$$G = G_0 \exp\left[-\frac{U^*}{R(T_c - T_\infty)}\right] \exp\left[-\frac{K_g}{T_c \Delta T f}\right]. \tag{3}$$

In eq. (3), G_0 is the pre-exponential factor, U^* the transport activation energy usually at 6300 J/mol, T_∞ a hypothetical temperature defined as $T_g - 30$, T_c the crystallization temperature, ΔT the degree of supercooling defined as $T_m^0 - T_c$, f a correction term to account for the variation in the bulk enthalpy of fusion calculated by $2T_c/(T_m^0 + T_c)$, and K_g a nucleation parameter expressed as follows:

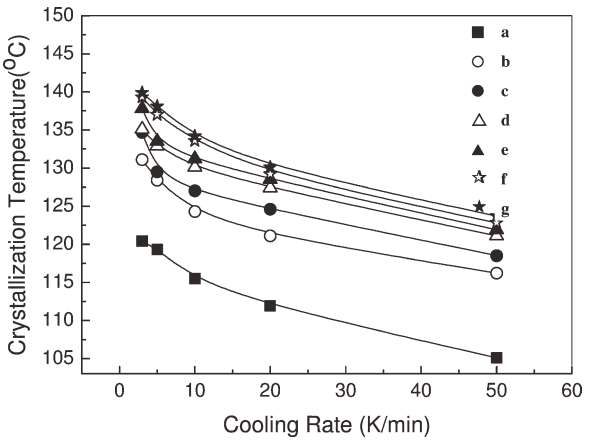

Figure 7. Effect of the cooling rate on the crystallization temperature corresponding to the maximum crystallization rate. (a) Neat MIPP, (b) M-1, (c) P-1, (d) M-2, (e) P-2, (f) M-3, and (g) P-3.

$$K_g = \frac{nb_0\sigma\sigma_e T_m^0}{\Delta h_f^0 k}, \tag{4}$$

where, for iPP, n, Δh_f^0, and b_0 are known to be 4, 1.34×10^8 J/m^3, and 6.56×10^{-10} m, respectively, k is the Boltzmann constant, σ_e the folding surface free energy, and σ the lateral surface free energy, which can be deduced by $\sigma = ab_0\Delta h_f^0$ (a $\approx$ 1). As the crystal growth rate can be calculated through $G = 1/t_{1/2}$,[29] eq. (3) can be expressed as follows:

$$\ln(t_{1/2})^{-1} + \frac{U^*}{R(T_c - T_\infty)} = \ln G_0 - \frac{K_g}{T_c \Delta T f}. \tag{5}$$

Figure 5 plots $\ln(t_{1/2})^{-1} + \frac{U^*}{R(T_c - T_\infty)}$ versus $\frac{1}{T_c \Delta T f}$, from where the K_g and then the chain folding free energy σ_e values are obtained. The results are summarized in Table III. The lower the folding free energy is, the less the energy consumed for polymer chain to fold on the nuclei surface to form spherulite. The systematically lower values of σ_e for P-series composition samples when compared with their M-series counterparts indicate that in the polymerization-rendered MIPP/DMBS compositions polymer chain is easier to fold and then crystallize on nuclei surface. This assumption is consistent with the outcome of the above discussion about the crystallization half-time $t_{1/2}$ and crystallization rate constant K.

Nonisothermal crystallization studies were also performed. Figure 6 presents all the recorded DSC scan trails, from where important parameters such as crystallization peak temperature (T_p) and relative crystallinity (X_t) are obtained. As expected, increasing the cooling rate caused a downward shift of T_p. Figure 7 draws the curves of crystallization temperature as a function of cooling rate for both series of MIPP/DMBS composition

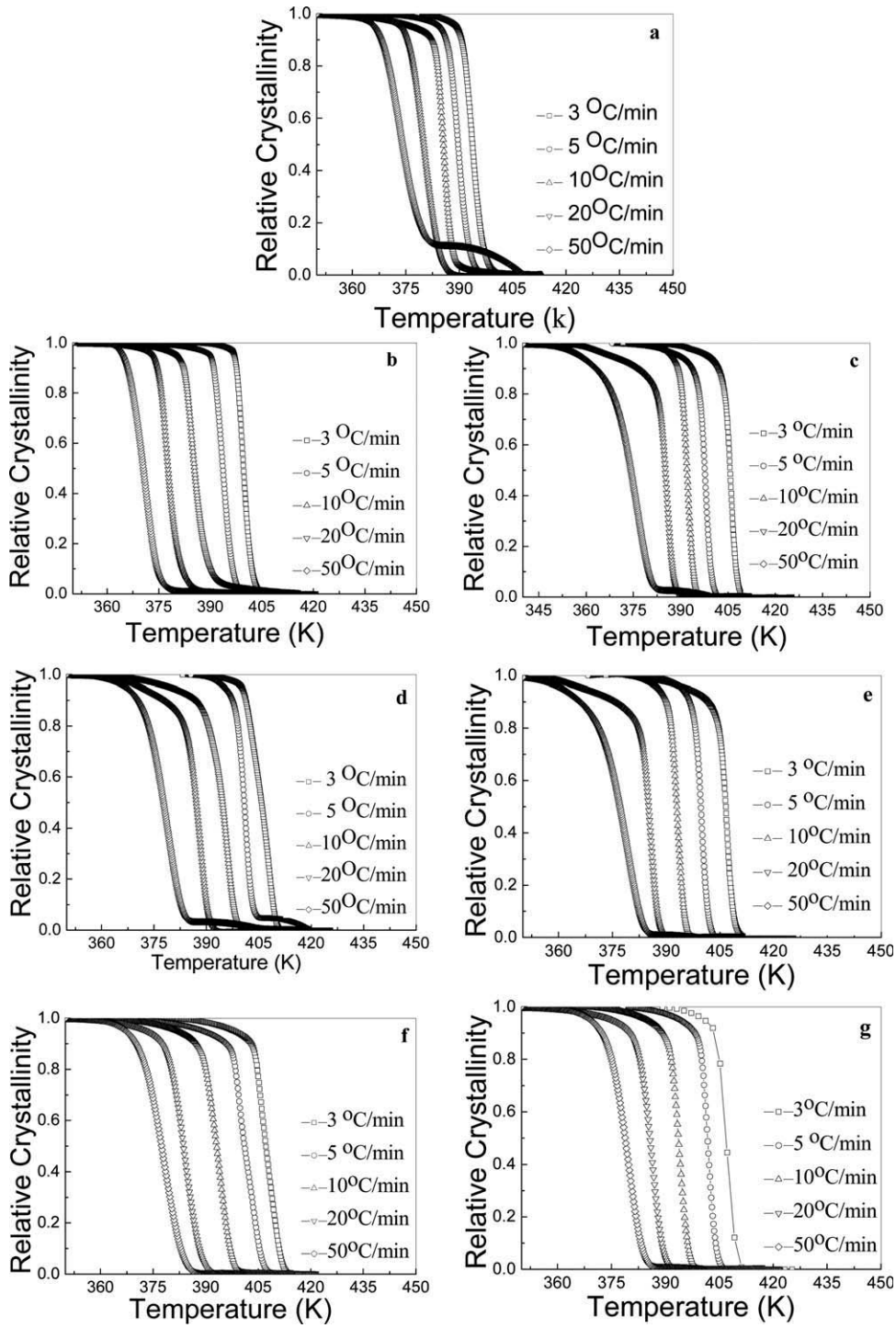

Figure 8. Plots of X_t versus T for crystallizations of (a) neat MIPP, (b) M-1, (c) P-1, (d) M-2, (e) P-2, (f) M-3, and (g) P-3.

polymers and the neat MIPP. Leaving the MIPP alone, clearly, the P-series composition polymers possess systematically higher crystallization temperatures than their M-series counterparts. This result is consistent with that of the isothermal crystallization study.

The relative degree of crystallinity, X_t, is defined as follows:

$$X_t = \int_{T_0}^{T} (dH_c/dT)dT \Big/ \int_{T_0}^{T_\infty} (dH_c/dT)dT, \qquad (6)$$

where T_0 and T_∞ are the onset and end of crystallization temperatures, respectively. Figure 8 shows the curves of the relative degree of crystallinity, X_t, as a function of temperature for all

Applied Polymer SCIENCE

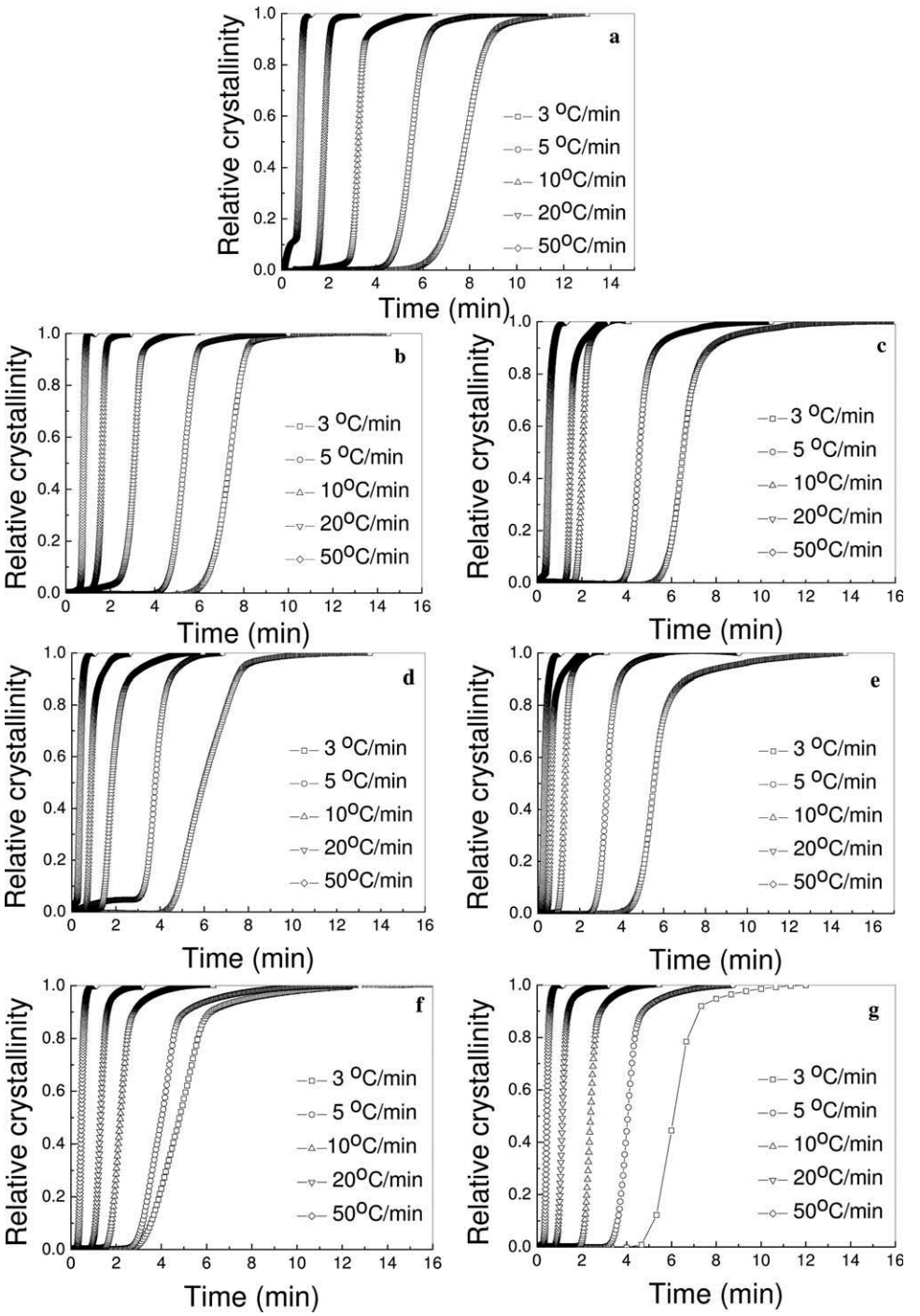

Figure 9. Plots of X_t versus t for crystallization of (a) neat MIPP, (b) M-1, (c) P-1, (d) M-2, (e) P-2, (f) M-3, and (g) P-3.

Table IV. Nonisothermal Crystallization Parameters of Neat MIPP and the Two Sets of MIPP/DMBS (both P- and M-Series) Compositions

	$t_{1/2}$ (min)							T_p (°C)						
λ (K/min)	Neat MIPP	M-1	P-1	M-2	P-2	M-3	P-3	Neat MIPP	M-1	P-1	M-2	P-2	M-3	P-3
3	7.8	7.4	6.5	6.0	5.5	4.8	4.3	120.4	131.1	134.7	135.1	137.8	139.3	139.9
5	5.5	5.3	4.6	3.8	3.3	3.0	2.8	119.3	128.4	129.5	132.9	133.5	137.0	138.1
10	3.3	3.1	2.0	1.8	1.3	1.2	1.0	115.5	124.3	127.0	130.1	131.2	133.6	134.2
20	1.8	1.6	1.1	0.9	0.7	0.6	0.5	111.9	121.1	124.6	127.4	128.5	129.2	130.1
50	0.8	0.7	0.5	0.4	0.3	0.2	0.2	105.1	116.2	118.5	121.1	121.9	122.0	123.7

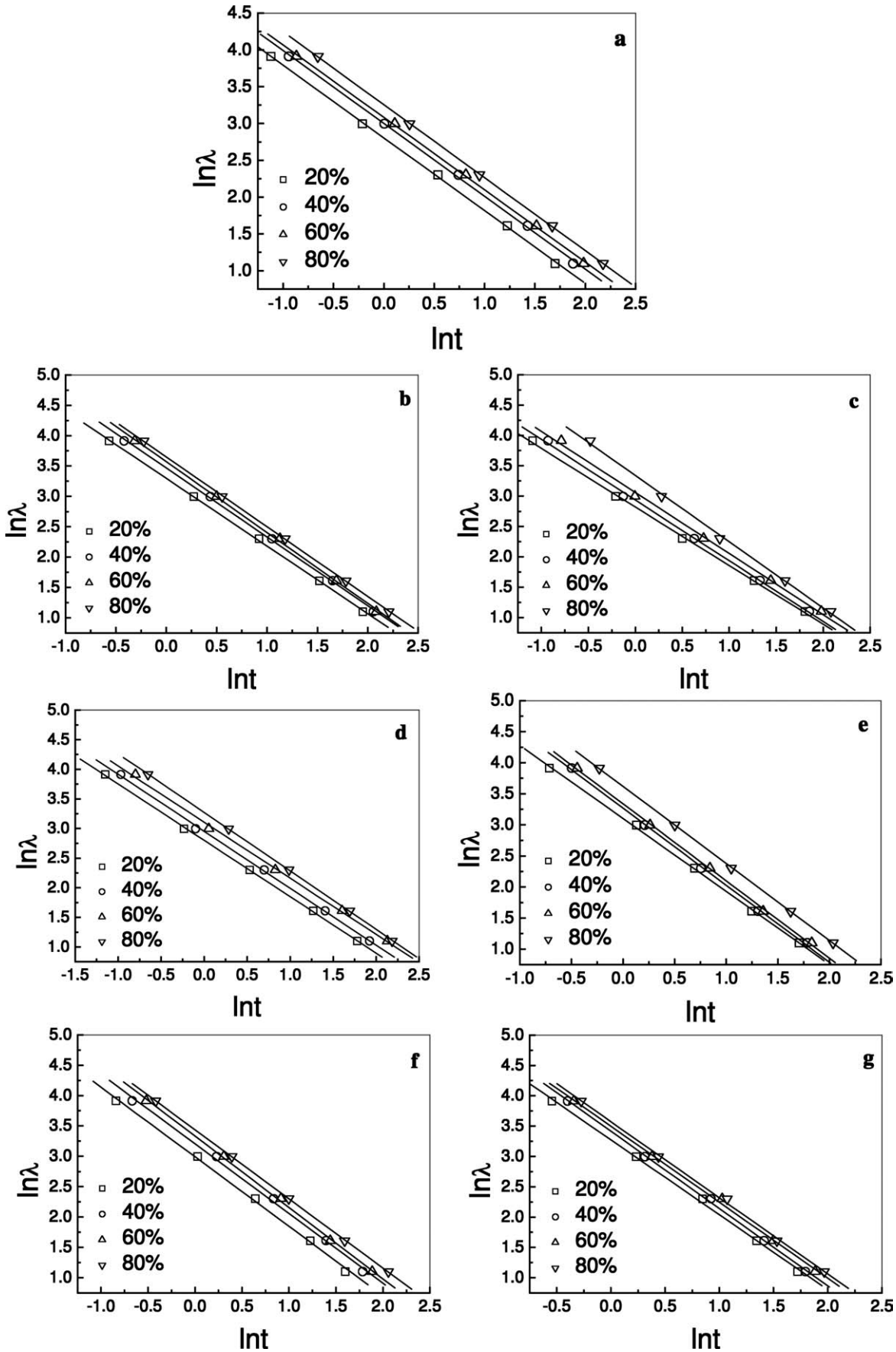

Figure 10. Plots of ln λ versus ln(t). (a) Neat MIPP, (b) M-1, (c) P-1, (d) M-2, (e) P-2, (f) M-3, and (g) P-3.

Applied Polymer SCIENCE

Table V. Values of $F(T)$, α, and ΔE for Neat MIPP and the Two Sets of MIPP/DMBS (both P- and M-Series) Compositions

Sample	X_t (%)	α	$F(T)$	ΔE (KJ/mol)
Neat MIPP	20	1.24	2.55	256.0
	40	1.27	3.04	
	60	1.25	3.30	
	80	1.26	3.56	
M-1	20	1.11	2.30	217.8
	40	1.13	2.80	
	60	1.17	3.06	
	80	1.15	3.19	
P-1	20	1.01	1.68	202.0
	40	1.00	1.88	
	60	0.97	2.13	
	80	1.04	2.82	
M-2	20	1.17	1.43	176.1
	40	1.24	1.63	
	60	1.24	1.82	
	80	1.24	2.33	
P-2	20	0.95	1.35	150.1
	40	0.96	1.52	
	60	0.95	1.74	
	80	0.99	2.14	
M-3	20	1.15	1.35	151.2
	40	1.15	1.41	
	60	1.18	1.70	
	80	1.14	2.11	
P-3	20	0.99	1.25	136.6
	40	0.99	1.31	
	60	0.98	1.58	
	80	0.99	1.99	

samples. All the curves have a sigmoidal shape. Using an equation of $t = (T_0 - T)/\lambda$ (where T is the temperature at crystallization time t and λ the cooling rate), the abscissa of temperature in Figure 8 is transformed into a timescale (Figure 9). The higher the cooling rate is, the shorter the time needed for completing the crystallization. The half-time of nonisothermal crystallization $t_{1/2}$ is estimated from Figure 9, the results being listed in Table IV. Once again, the P-series samples show systematically lower $t_{1/2}$s than their M-series counterparts, which is also in good agreement with that of the isothermal crystallization study.

The nonisothermal crystallization kinetics data were processed using Mo's method with the following equation[30]:

$$\ln \lambda = \ln F(T) - \alpha \ln(t), \tag{7}$$

where $F(T) = [K(T)/k]^{1/m}$ refers to the cooling rate that needs to be selected within a unit of crystallization time when measured system amounts to a certain degree of crystallinity, and α is the ratio of Avrami exponent n to Ozawa exponent m (n/m).[31] The smaller the value of $F(T)$, the higher the crystallization rate becomes. Figure 10 draws the plots of ln λ versus ln(t) at different crystallinities, where the values of α and $F(T)$ were derived as the slope and intercept of the linear fitting. The results are listed in Table V. As the deviations of α values among the samples are quite small, eq. (7) was eligible to describe the nonisothermal crystallization behaviors. As is seen in Table V, $F(T)$ increases with increasing relative crystallinity, indicating that at a unit crystallization time, a higher cooling rate is required to obtain higher degree of crystallinity. These results are also consistent with the literature findings,[32,33] as are the isothermal crystallization results. A side-by-side comparison of $F(T)$ values between the two series of MIPP/DMBS composition polymers clearly shows that the P-series samples are of systematically higher crystallization rates compared with their M-series counterparts.

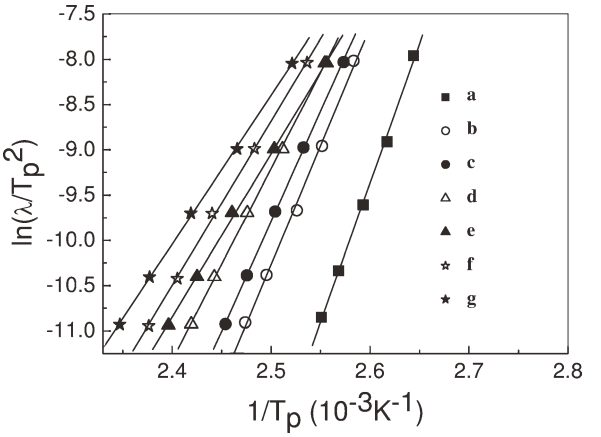

Figure 11. Kissinger plots for evaluating nonisothermal crystallization activation energies. (a) Neat MIPP, (b) M-1, (c) P-1, (d) M-2, (e) P-2, (f) M-3, and (g) P-3.

It is known that the crystallization of polymers is controlled by two factors: the dynamic factor, related to the ΔE for the transport of crystalline units across the phase, and the static factor, related to the free energy barrier for nucleation. The ΔE for nonisothermal crystallization can be evaluated by Kissinger

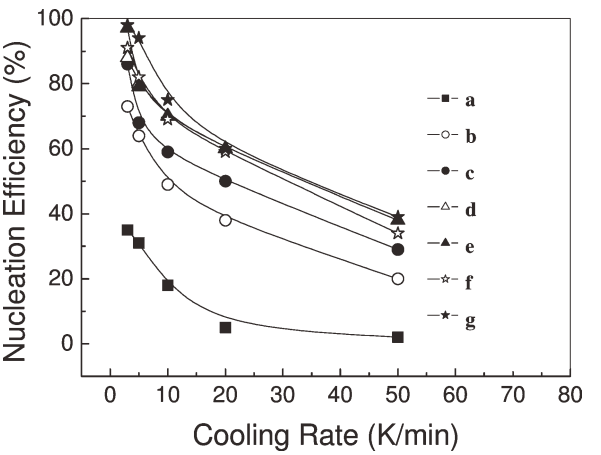

Figure 12. Nucleation efficiencies for (a) neat MIPP, (b) M-1, (c) P-1, (d) M-2, (e) P-2, (f) M-3, and (g) P-3.

method.[34] Taking into account the variation of the peak temperature T_p with the cooling rate λ, the effective activation energy ΔE can be evaluated using the following equation:

$$\frac{d[\ln \phi/T_p^2]}{d(1/T_p)} = -\frac{\Delta E}{R}, \quad (8)$$

where R is the gas constant. Figure 11 dots the $\ln(\lambda/T_p^2)$ versus $1/T_p$ for all the samples with linear fitting. All linear fittings are of high regression coefficients. Their slopes give the effective activation energy ΔE, which are listed in Table V. As can be seen, the ΔE values for the P-series MIPP/DMBS composition polymers are not only lower than that of the neat MIPP but also significantly lower than those of their M-series counterparts.

Finally, the nucleation efficiencies of DMBS in the two sets of composition polymers under nonisothermal crystallization conditions were evaluated and compared one another as well as with the neat MIPP. According to Lotz and coworkers,[35] a nucleation efficiency is expressed as follows:

$$N_E = \frac{T_c - T_{c,\text{lower}}}{T_{c,\text{upper}} - T_{c,\text{lower}}} \times 100, \quad (9)$$

where $T_{c,\text{lower}}$ and $T_{c,\text{upper}}$ are the crystallization temperatures of a neat, nonnucleated iPP and a best self-nucleated iPP, respectively, and T_c is the crystallization temperature of the concerned nucleated PP sample. N_E is thus 0 for a nonnucleating action and 100 for the maximum efficiency. Jain et al.[36] determined the values of $T_{c,\text{lower}}$ and $T_{c,\text{upper}}$ for iPP by DSC, which turned out to be 110.6 and 138.6°C, respectively. With eq. (9), nucleation efficiencies for MIPP/DMBS composition and neat MIPP samples during nonisothermal crystallization at different cooling rates are estimated and summarized in Figure 12. Obviously, MIPP/DMBS composition polymers exhibit much higher nucleation efficiencies, regardless of their fabrication techniques. Especially at some very low cooling rates, the nucleation efficiencies of the composition polymers can easily go up to 70% and up, whereas those of the neat MIPP reach no more than 35%. Nucleation efficiencies in general decrease with increasing cooling rates. Interestingly, although significant differences are not observed between the two types of composition polymers at low cooling rates, clearly higher nucleation efficiencies are discernible for the P-series MIPP/DMBS compositions over their M-series counterparts at high cooling rates, and, more interestingly, the lower the DMBS concentration, the larger the nucleation efficiency gap between the P-series and M-series compositions. For instance, at a cooling rates of 50 k/min, which resembles an ambient cooling process, MIPP/DMBS compositions containing 0.31 and 0.52 wt % of DMBS show only marginal differences of nucleation efficiency between P and M samples; however, a percentage gap close to 10% is found when comparing the two composition polymers containing 0.22 wt % of DMBS, the nucleating agent, with the nucleation efficiency of the P sample (38%) close to that of a M sample containing the highest level of DMBS of 0.52% (40%). These results may be ascribed to the polymerized compounding technique that might not only greatly promote the dispersion homogeneity of the nucleating agent but also reduce the crystallization free energy because of an enhanced interfacial compatibility between the exotic nuclei and the PP matrix.

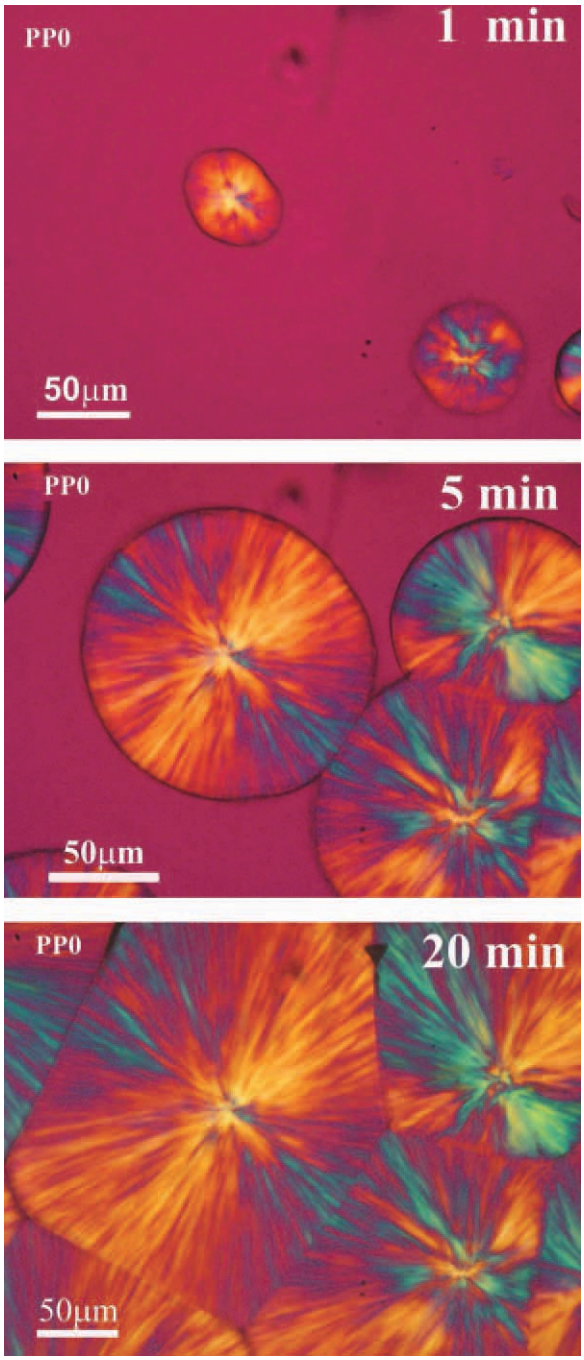

Figure 13. Evolution of the spherulites of neat MIPP during isothermal crystallization at 140°C. [Color figure can be viewed in the online issue, which is available at wileyonlinelibrary.com.]

POM Study

POM images of the neat MIPP and the two series of MIPP/DMBS composition polymers isothermally crystallized at 140°C for varied times are shown in Figures 13–15, respectively. It is

Applied Polymer SCIENCE

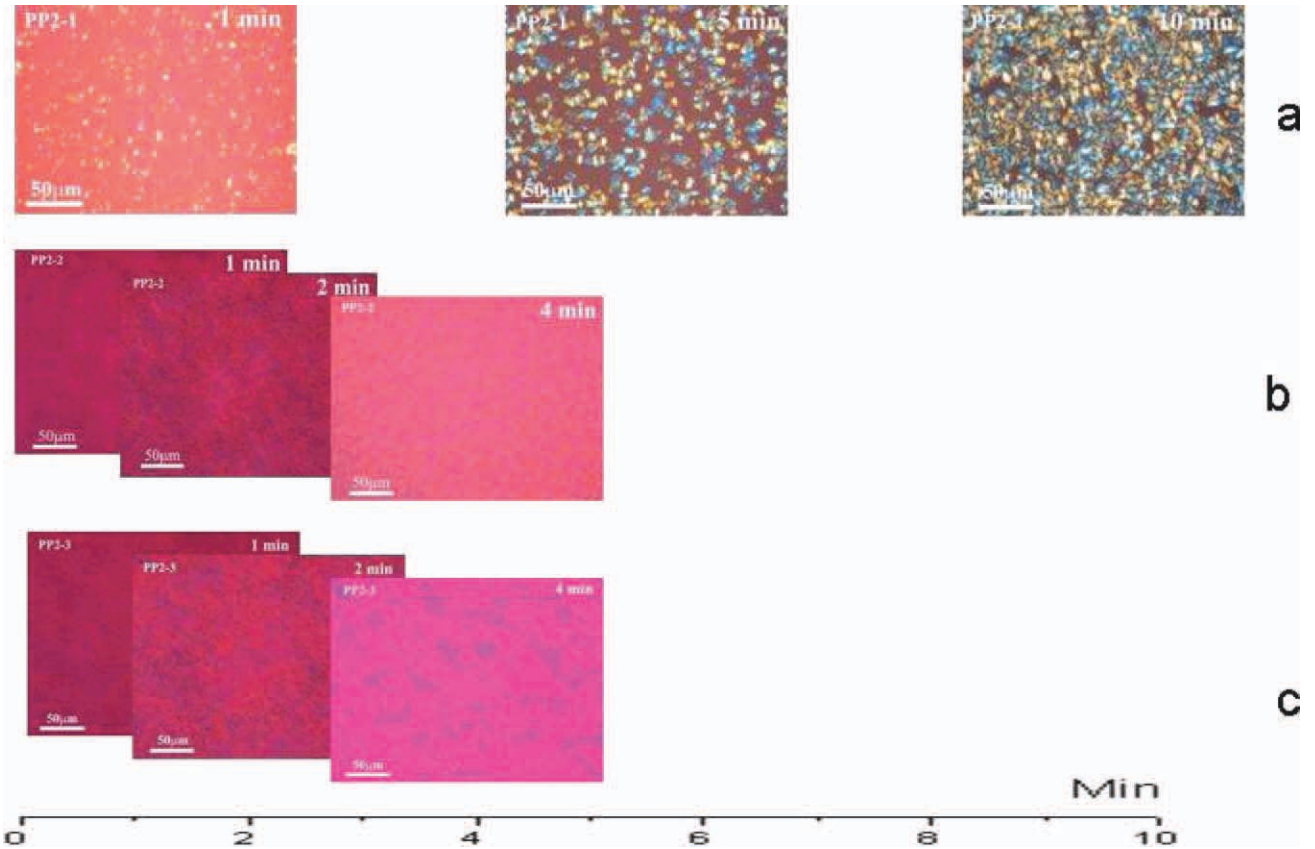

Figure 14. Evolution of the spherulites of MIPP/DMBS melt-mixed compositions during isothermal crystallization at 140°C. (a) M-1, (b) M-2, and (c) M-3. [Color figure can be viewed in the online issue, which is available at wileyonlinelibrary.com.]

clearly seen that the addition of DMBS, the nucleating agent, into MIPP, whatever method (polymerization or melt mixing) was adopted, not only expedited the overall crystallization process but also profoundly reduced the average size of the crystal spherulites; the more the nucleating agent being loaded, the faster the crystallization and the smaller the average crystallite size. However, what is really interesting is that, in contrast to the hardly discernible differences between the crystal morphologies of the P- and M- series compositions containing some relatively higher DMBS contents of 0.31 and 0.52 wt %, the evolutions of crystallization of the two lower DMBS-loaded compositions containing 0.21 wt % of DMBS show distinctive differences, the P sample exhibiting considerably more nuclei than its M counterpart in the very beginning of crystallization and no sluggish in the subsequent crystal growth, thus leading to faster crystallization and apparently higher crystallinity and forming much finer crystallites. This is ascribable to the more efficient DMBS dispersion and better affinity between the nucleating agent and iPP matrix caused by a polymerized compounding than by the traditional melt mixing that is more profound at lower DMBS loading.

UV–Vis Spectroscopy Study

The total seven polymer samples, including the neat MIPP and the two series of MIPP/DMBS composition polymers, were all subjected to injection molding to prepare round plaque specimens of 1-mm thickness and 25-mm diameter for UV–vis spectrometer examination. Good consistency was achieved for the specimen preparation among the whole series of samples. The UV–vis spectroscopy experiment was carried out at ambient temperature with a scanning wavelength range between 400 and 700 nm. The results are illustrated in Figure 16, where the acquired absorption data of the two series of MIPP/DMBS composition polymer samples are normalized with respect to those of the neat MIPP giving comparison-friendly relative absorption curve for each sample. It is evident that the nucleating indeed improved the clarity of iPP, as the relative absorbance of all the composition samples is negative in the entire span of 400 and 700 nm and shows a decreasing trend with the decrease of the incident beam wavelength from 700 to 400 nm, indicative of reduced crystal spherulite size. Side-by-side comparing the relative absorption curves between the two series of MIPP/DMBS composition samples gives a general impression that the P-series samples are of systematically better clarity than their M-series counterparts, which is in accord with the results from both the DSC and POM studies showing enhanced nucleating efficiency of the P-series MIPP/DMBS compositions when compared with that of the M-series samples. However, a more scrutinous examination of the absorption data pertinent to the two series of composition samples reveals that the advantage in clarity improvement brought by a polymerized compounding of the nucleated compositions over the traditional melt-mixing

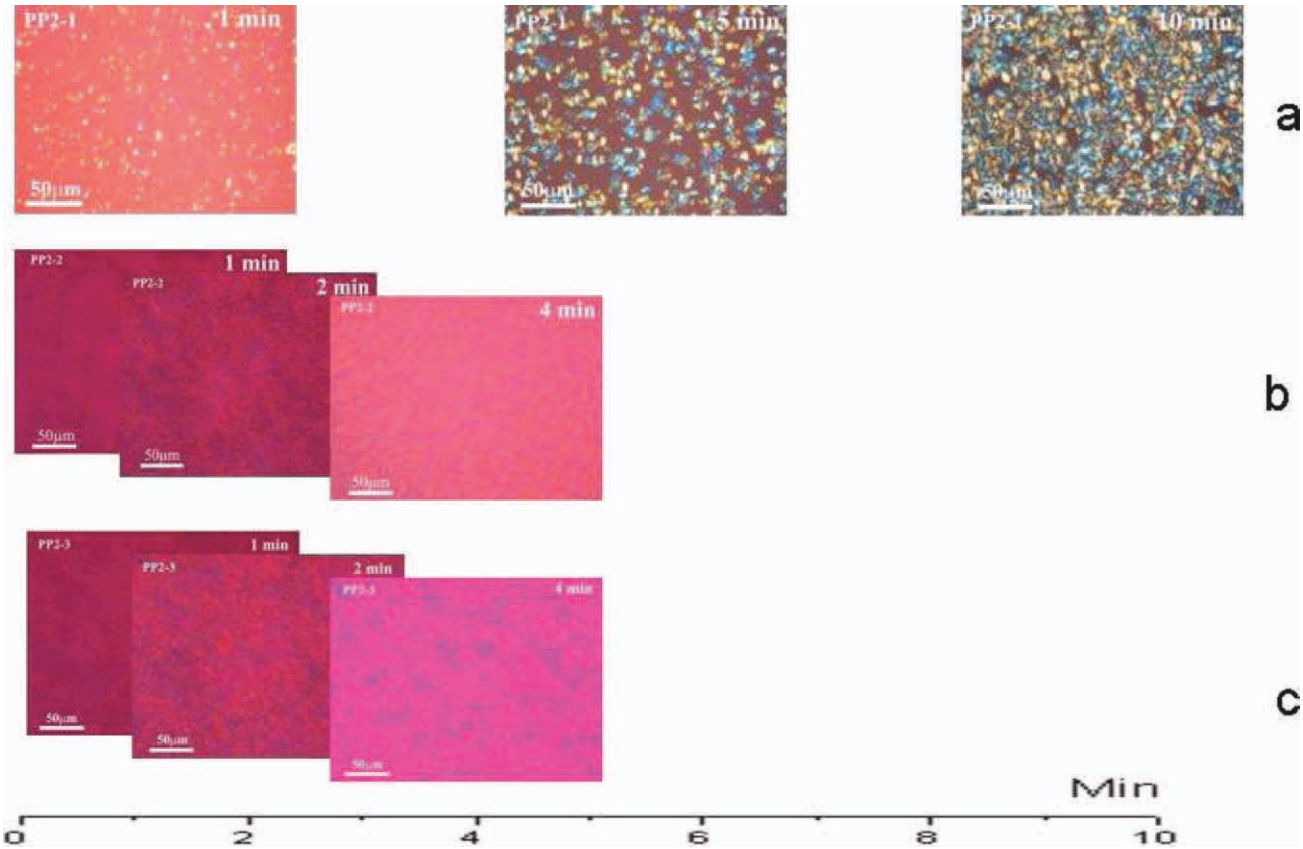

Figure 15. Evolution of the spherulites of MIPP/DMBS melt-mixed compositions during isothermal crystallization at 140°C. (a) P-1, (b) P-2, and (c) P-3. [Color figure can be viewed in the online issue, which is available at wileyonlinelibrary.com.]

compounding is insignificant when the DMBS, the nucleating agent, content in the composition is at some higher levels of 0.31 and 0.53 wt %; nevertheless, at a DMBS content of 0.22 wt %, the lowest nucleating agent loading among the three DMBS weight percentage levels, the P sample exhibits the most significant jump from the M sample, which shows a relative absorption curve only marginally different from the normalized line.

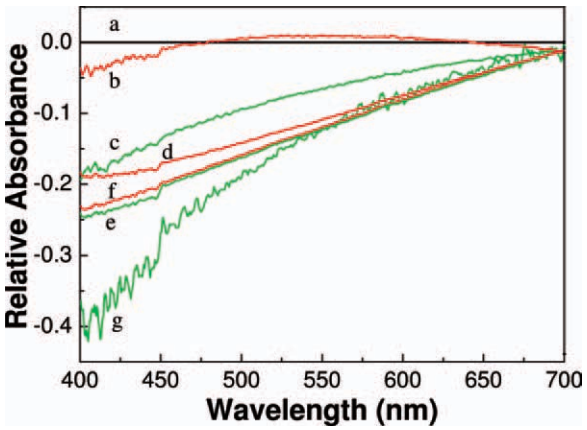

Figure 16. Relative UV absorbance normalized to neat MIPP. (a) Neat MIPP, (b) M-1, (c) P-1, (d) M-2, (e) P-2, (f) M-3, and (g) P-3. [Color figure can be viewed in the online issue, which is available at wileyonlinelibrary.com.]

In fact, the P sample containing 0.22 wt % of DMBS demonstrates an absorption curve very close to that of an M sample containing 0.31 wt % of DMBS.

CONCLUSION

In this article, we investigated the effect of a polymerized compounding method on the nucleation behavior of a sorbitol derivative nucleating agent in the melt crystallization of iPP. By using a sorbitol derivative nucleating agent, DMBS, which displays itself as aggregated fibrillar crystals, as a support for C_2-symmetric *ansa*-metallocene of *rac*-Me_2Si[2-Me-4-Naph-Ind]$_2ZrCl_2$, propylene polymerization *in situ* resulted in the formation of iPP/DMBS composition polymers having controllable DMBS concentrations, with the DMBS dispersion driven by catalyst fragmentation. Three iPP/DMBS composition polymers having DMBS concentrations of 0.22, 031, and 0.52 wt % were prepared by this means, which, along with their analog melt-mixed counterparts, were subjected to melt crystallization kinetics and crystal morphology studies using DSC, POM, and UV–vis spectroscopy. Some general advantages of the polymerized compounding of iPP/DMBS nucleating agent compositions over a traditional melt-mixing compounding in terms of the effectiveness for the nucleating agent to influence iPP crystallization were revealed, which include enhanced nucleation efficiency and reduced crystallization free energy, both of which facilitated iPP crystallization by expediting the overall

crystallization process and decreasing the crystallite dimension. More specifically, the advantage of a polymerized compounding is more prominent at low nucleating agent loadings than at high loadings.

ACKNOWLEDGMENTS

Financial support by the National Science Foundation of China (Grant nos. 20734002 and 20874104), Ministry of Science and Technology of China (863 project, series nos. 2008AA030901 and 2009AA033601), and Chinese Academy of Sciences (Directional Key Project on High-Performance Polypropylene Alloy Resin Development) is gratefully acknowledged.

REFERENCES

1. Galli, P.; Vecellio, G. J. *J. Polym. Sci. Part A: Polym. Chem.* **2004,** *3*, 396.
2. Shepard, T. A.; Delsorbo, C. R.; Louth, R. M.; Walborn, J. L.; Norman, D. A.; Harvey, N. G.; Spontak, R. J. *J. Polym. Sci. Part B: Polym. Phys.* **1997,** *35*, 2617.
3. Kristiansen, M.; Tervoort, T.; Smith, P. *Macromolecules* **2005,** *38*, 10461.
4. Smith, T. L.; Masilaman, D. M.; Bui, L. K.; Khanna, Y. P.; Bray, R. G.; Hammond, W. B.; Curran, S.; Belles, J. J.; Bider-Castelli, S. *Macromolecules* **1994,** *27*, 3147.
5. Feng, Y.; Jin, X.; Hay, J. N. *J. Appl. Polym. Sci.* **1998,** *69*, 2089.
6. Phillips, R.; Manson, J. E. *J. Polym. Sci. Part B: Polym. Phys.* **1997,** *35*, 875.
7. Kim, Y. C.; Kim, C. Y.; Kim, S. C. *Polym. Eng. Sci.* **1991,** *31*, 1009.
8. Lipp, J.; Shuster, M.; Terry, A. E.; Cohen, Y. *Langmuir* **2006,** *22*, 6398.
9. Dong, X. C.; Wang, L. J. Phys. Chem. *B* **2006,** *236*, 145.
10. Yuksekkalayci, C.; Yilmazer, U.; Orbey, N. *Polym. Eng. Sci.* **1999,** *39*, 1216.
11. Xiang, C.; Sue, H. J.; Chu, J.; Masuda, K. *Polym. Eng. Sci.* **2001,** *41*, 23.
12. Karger-Kocsis, J.; Varga, J.; Ehrenstein, G. W. *J. Appl. Polym. Sci.* **1997,** *64*, 2057.
13. Libster, D.; Aserin, A.; Gerti, N. *J. Colloid Interface Sci.* **2006,** *299*, 172.
14. Libster, D.; Aserin, A.; Gerti, N. *J. Colloid Interface Sci.* **2006,** *302*, 322.
15. Zhang, Y. F.; Xin, Z. *J. Polym. Sci. Part B: Polym. Phys.* **2007,** *45*, 590.
16. Zhu, W. P.; Zhang, G. P.; Yu, J. Y.; Dai, G. *J. Appl. Polym. Sci.* **2004,** *91*, 431.
17. Yi, Q. F.; Wen, X. J.; Dong, J. Y.; Han, C. C. *Macromol. React. Eng.* **2007,** *1*, 307.
18. Macauley, N. J.; Harkin-Jones, E. M. A.; Murphy, W. R. *Polym. Eng. Sci.* **1998,** *38*, 516.
19. Beck, H. N. *J. Appl. Polym. Sci.* **1967,** *11*, 673.
20. Spaleck, W.; Kuber, F.; Winter, A.; Rohrmann, J.; Bachmann, B.; Antberg, M.; Dolle, V.; Paulus, E. F. *Organometallics* **1994,** *13*, 954.
21. Avrami, M. J. *J. Chem. Phys.* **1939,** *7*, 1103.
22. Hoffman, J. D. *Polymer* **1983,** *24*, 3.
23. Zhang, Y. F.; Li, X.; Wei, X. S. *J. Macromol. Sci. Part B: Phys.* **2008,** *47*, 891.
24. Nagarajan, K.; Levon, K.; Myerson, A. S. *J. Therm. Anal. Calorim.* **2000,** *59*, 497.
25. Marco, C.; Ellis, G.; Gomez, M. A.; Arribas, J. M. *J. Appl. Polym. Sci.* **2003,** *88*, 2261.
26. Kowalewski, T.; Galeski, A. *J. Appl. Polym. Sci.* **1989,** *32*, 2919.
27. Lopez-Manchado, M. A.; Biagiotti, J.; Torre, L.; Kenny, J. M. *Polym. Eng. Sci.* **2000,** *40*, 2194.
28. Hoffman, J. D.; Miller, R. L. *Polymer* **1997,** *38*, 3151.
29. Lauritzen, J. I.; Hoffman, J. D. *J. Appl. Phys.* **1973,** *44*, 4340.
30. Liu, T. X.; Mo, Z. S. *Acta Polym. Sin.* **1993,** *1*, 1.
31. Ozawa, T. *Polymer* **1971,** *12*, 150.
32. Zhang, Y. F.; Li, X.; Wei, X. S. *J. Therm. Anal. Calorim.* **2010,** *100*, 661.
33. Dobreva, T.; Lopez-Majada, J. M.; Perena, J. M.; Perez, E.; Benavente, R. *J. Appl. Polym. Sci.* **2008,** *109*, 1338.
34. Kissinger, H. E. *J. Res. Natl. Inst. Stand.* **1956,** *57*, 217.
35. Fillon, B.; Thierry, A.; Lotz, B.; Wittman, J. C. *J. Therm. Anal.* **1994,** *42*, 721.
36. Jain, S.; Goossens, H.; Lemstra, P. *Polymer* **2005,** *46*, 8805.